J Mater Sci: Mater Electron (2016) 27:8325–8331
DOI 10.1007/s10854-016-4841-6

Influence of polyimide on thermal stress evolution in polyimide/Cu thick film composite

Heng Li[1,2] · Gong Cheng[1,2] · Gaowei Xu[1] · Le Luo[1]

Received: 27 February 2016 / Accepted: 15 April 2016 / Published online: 29 April 2016
© Springer Science+Business Media New York 2016

Abstract Polyimide(PI)/Cu composite thick films are widely used in wafer level packaging (WLP), and a common problem is the defects such as void, delamination, crack or wafer warpage induced by thermal stress. Compared with traditional rigid substrate/Cu/passivation system, PI imposes quite a different boundary constraint on Cu, resulting in a special stress evolution, and the corresponding mechanism is far from fully understood. Five sets of composites are constructed to investigate the influence of PI on thermal stress evolution in Cu film by means of in situ wafer warpage measurement under thermal cycling. Together with finite element analyses, it's counterintuitive to find that although PI indeed reduces the stress in Cu, it exacerbates overall wafer warpage at room temperature. Warpage evolution reveals that composites consisting of substrate/PI/Cu sustains a moderate compressive stress while bare PI film is totally stress relaxed at high temperature, indicating that Cu and PI restrains stress relaxation reciprocally. It suggests that mutual effect should be considered when evaluating the stress distribution in polymer-metal composite thick films.

✉ Le Luo
leluo@mail.sim.ac.cn

[1] State Key Laboratory of Transducer Technology, Shanghai Institute of Microsystem and Information Technology, Chinese Academy of Sciences (CAS), Shanghai 200050, China

[2] University of Chinese Academy of Sciences, Beijing 100049, China

1 Introduction

Polymer/metal composite thick films are widely used in wafer level packaging (WLP). A common problem of such composites is the thermal stress when undergo packaging process in which the induced undesirable thermal stresses and corresponding microstructure evolution might cause void, hillock, crack or interfacial delamination in layered structures [1, 2]. Moreover, large wafer warpage originated from Cu and PI deformation poses a threat to handling of the wafer and affects the quality of sequential process steps such as lithography [3–5]. Stress evolution of Cu films due to coble creep, power-law creep, dislocation glide/climb, or grain growth has been analyzed [6–17], and transient behavior and Bauschinger-like Effect also draw the attention of industry people [12, 18].

The polymer has large influence on stress relaxation of metals within composites due to sophisticated reaction during curing process and thermal cycling [19–28]. Various polymers, including polyimide resin, cyanate ester resin, bismaleimide resin, benzoxazine resin and so on, have been widely studied [29–33]. Typically, polyimide (PI) is widely used in semiconductor industry for passivation or dielectric layer. Due to dramatic elution of thermal mechanical properties during curing process, large stress may arise in the composites. Figure 1 depicts some typical thermal stress induced defects in a 2P1 M (two PI layers with one metal layer embedded) composite from our research project, which is commonly used in redistribution layer (RDL) in WLP. The defects include PI crevices within one PI layer caused by intrinsic stress, delamination at PI/Cu interface caused by coefficient of thermal expansion (CTE) mismatch,and cracks at the interface of two PI layers caused by shrinkage.

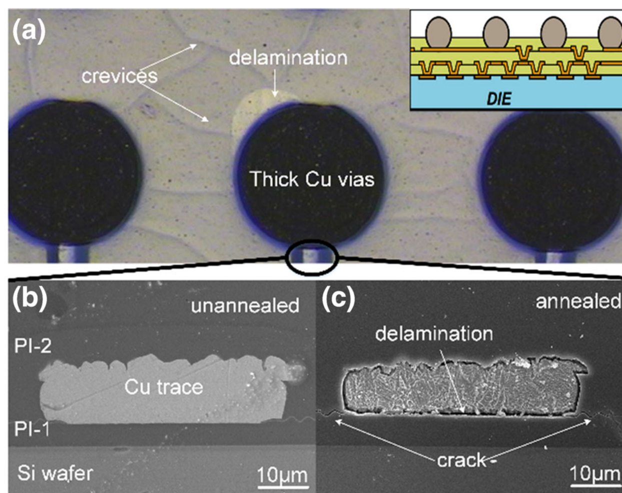

Fig. 1 Thermal stress induced typical defects in PI/Cu composite. **a** is an optical image from top view, with an *inset* schematically illustrating the composites in RDL. **b**, **c** are SEM images of annealed and annealed 2P1 M respectively

In polymer/metal composites, the mechanism of stress evolution is far from fully understood. Polymers usually imposes a soft constrains, which is rather different from rigid constrains, such as Si wafer substrate or inorganic passivation. In PI/Cu composites, the PI beneath the Cu film cannot prevent dislocations in Cu from gliding at PI/Cu interface, which differs from Si wafer substrate in constrained diffusional creep model [9]. Also, the PI coated above Cu film is not an effective passivation for surficial diffusion of Cu atoms when compared with other oxide or nitride or metal passivation layer. Hence, some traditional models, such as constrained diffusional creep, cannot evaluate the stress evolution process of the composite satisfactorily [9, 17, 34].

In this work, five sets of PI/Cu composites are investigated by warpage measurement. The influence of PI on wafer warpage, as well as its influence on stress distribution and evolution within Cu/PI composite thick films are experimentally analyzed.

2 Experimental

The stress evolution in PI/Cu composite during thermal cycling is analyzed on a 4-inch 420 μm-thick double-polished (DSP) (100) silicon wafer substrate.

PI used in this work is solvent developable negative-tone photo-definable polyimide (PDPI) HD-4100 from HD microsystem, which is widely used in semiconductor industry for passivation, RDL or dielectric layers. The solvent is *N*-methyl-2-pyrrolidone. The impurity content of chloride, sodium, potassium, copper, iron are less than 1.0 ppm respectively, and the total metals are less than 10.0 ppm, as shown in Table 1.

It is spin coated onto the DSP wafer at a speed of 2000 rpm, then cured in the oven under nitrogen protection. The temperature profile of the curing process is shown in Fig. 2, i.e., heating from room temperature (RT) to 375 °C with a temperature rate of 10 °C/min, followed by cooling to RT gradually. To evaporate solvent adequately and to control the residual stress, the PDPI HD 4100 is isothermal annealed at 200 °C for 30 min and at 375 °C for 60 min. The isothermal annealing is important for the chemical reaction and solution evaporation, otherwise bubbles may arise and the cured film may be imperfect. The thickness of a single cured PI layer is10.10 ± 0.23 μm in current work.

The Cu film is electro-chemical deposited (ECD) on the DSP wafer, with the thickness of 5 μm. The plating system is from Technic (SEMCON^{TM}). Prior to Cu electroplating, a 100 nmTi/200nm Cu seedlayer is sputtering deposited by physical vapor deposition (PVD) in high vacuum continuously.

As illustrated in Fig. 3, five sets of samples are prepared on DSP wafers. In *set A* and *set B*, bare PI or Cu film are coated on the wafers. In *set C* ∼ *E*, the PI/Cu composites are also prepared. Specifically, in set C, the Cu film is electroplated on the wafer, and a PI layer is then spin coated above the Cu film and then cured. Such a PI layer is referred as capping PI, and this sample is referred as Si/Cu/PI. In *set D*, PI is firstly spin coated and cured onto the

Table 1 The properties of PDPI HD-4100 before and after cured in current work

Solution properties		Cured Film properties (typical data)	
Solids content (%)	33.2 ± 5.0	Decomposition temperature	600 °C
Viscosity (cSt)	3060 ± 660	Initial (1 %) weight loss	430 °C
Flash point	93 °C	Residual stress	34 MPa
Copper content	1.0 ppm max	Dielectric constant (1 MHz)	3.36
Iron content	1.0 ppm max	Surface resistivity (50 V)	3.3E16 Ω
Total metals	10.0 ppm max	Volume resistivity (50 V)	2.4E16 Ω
glass transition	280 °C	Dissipation factor (1 MHz)	0.001
Solvents	*N*-methyl-2-pyrrolidone	Dielectric strength	250 kV/mm

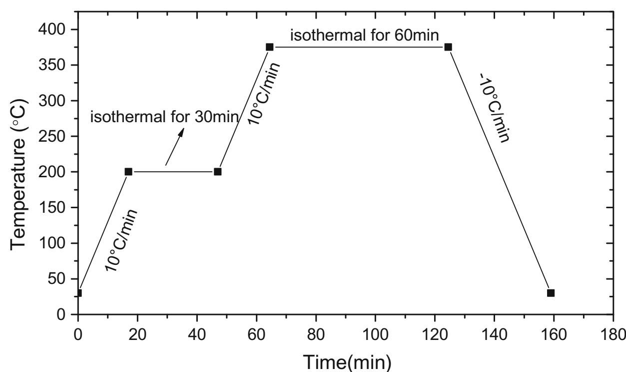

Fig. 2 The curing profile of PDPI HD4100 in current work

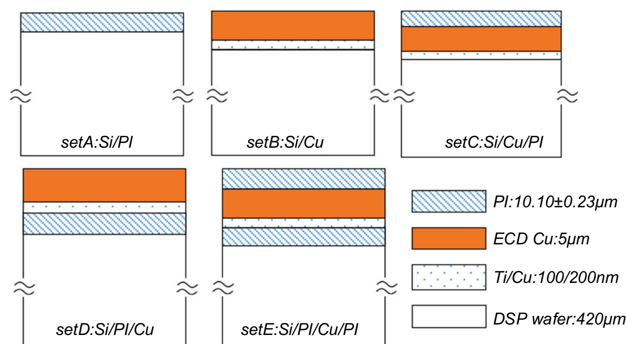

Fig. 3 Five sets of films consists of Cu and/or PI. All PI layers are 10.10 μm and all Cu layers are 5 μm thick

wafer, followed by the seedlayer deposited onto the PI layer, then Cu is electroplated on the seedlayer. Similarly, such a PI layer is called bottom PI, and this structure is referred as Si/PI/Cu. Finally, a Si/PI/Cu/PI structure is prepared by similar process, which is referred as 2P1 M and named as *set E*.

Wafer warpage evolution versus thermal cycling ($\kappa - T$) is in situ measured by a Multi-beam Optical Sensor (MOS) system from k-Space Associate Inc, based on the principle of laser reflection [35, 36]. The heating/cooling rate is 10 °C/min for PI and 5 °C/min for Cu unless otherwise specified. Only $\kappa - T$ curves of the second cycle is plotted in this work, because the curves is unstable until the 2nd cycle.

3 Results

3.1 $\kappa - T$ response of a single layered film

Figure 4 shows the measured results of single layered PI or Cu film. In Fig. 4b, the $\kappa - T$ curve is transferred into stress–strain ($\sigma - \varepsilon$) curve. Net stress σ_f, containing thermal stress component and intrinsic component, can be derived by a revised Stoney's Formula [37], and net strain is determined by CTE mismatch and warpage, as shown below:

$$\sigma_f = \sigma_0 + \frac{B_s t_s^3}{6t_f(t_f + t_s)}(\kappa - \kappa_0) \quad (1)$$

$$\varepsilon = \varepsilon_{thermo} + \varepsilon_{curv} = (\alpha_f - \alpha_s)(T - T_{ref}) - \kappa(t_f + t_s) \quad (2)$$

where κ, E, t and μ are measured curvature, Young's Modulus, thickness, and Poisson's ratio respectively. Biaxial modulus (effective Young's modulus) B can be defined as $B = E/(1 - \mu)$ for planner stress, and the subscript s and f refers to Si wafer substrate and composite films respectively. Material parameters are shown in

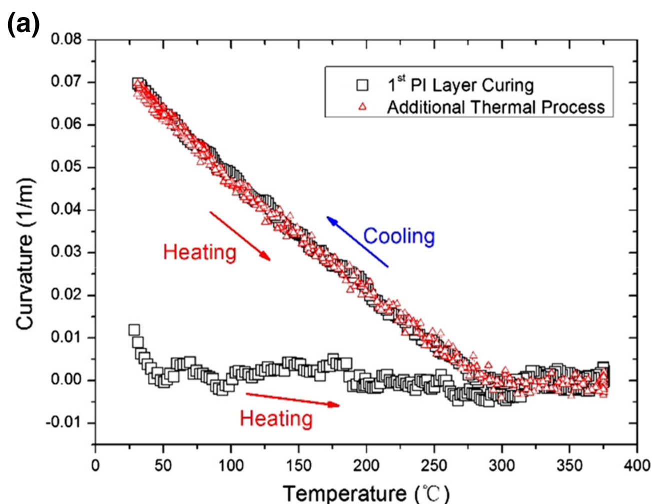

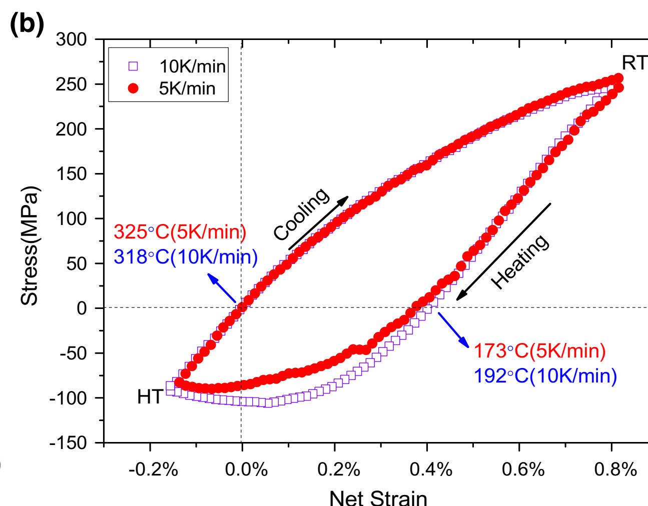

Fig. 4 The measured results of single layered films. **a** The $\kappa - T$ response of bare PI layer during first two cycles. **b** The $\sigma_f - \varepsilon$ curve of bare Cu film under different thermal rate

Table 2 Basic mechanical parameters of materials used in this work

	Biaxial modulus (GPa)	TCE (ppm/°C)	Poisson's ratio	CTE (ppm/°C)	Remarks
Si [38]	180	~−60	0.28	2.7	(100)DSP Si wafer,
Cu [39]	167	~−245	0.34	16.7	
PI [36]	4.99	~−2500	0.35	35	$T_g = 280$ °C, $\sigma_s = 200$ MPa elongation = 45 %

Table 2. To evaluate the temperature drift of the materials properties, the temperature coefficient of Young's Modulus (TCE) is also listed in the table. The TCE of PI is presented by storage modulus in dynamic mechanical analysis (DMA) test [36].

It is noted that bare PI film (*set A*) reveals linearity below T_g and viscoelasticity above T_g, and complete stress relaxation occurs without any compressive stress sustained at above 300 °C,showing an elastic behavior, while bare Cu film reveals hysteresis, with a stabilized loop from 250 MPa at RT to −100 MPa at high temperature(HT). As for the Cu films, the $\kappa - T$ curve with different thermal rate (10 and 5 K/min) is quite similar except the compressive range during heating, suggesting that the $\kappa - T$ response is not sensitive to temperature rate in current temperature range. At above 200 °C, stress relaxes occurs dramatically due to microstructural changes such as atom diffusion or grain growth (during the first cycle). Generally, in an unpassivated film, surficial diffusion occurs at lowest temperature, followed by grain boundary (GB) diffusion, and then dislocation/interface diffusion, and at last lattice diffusion (Nabarro-Herring creep) at highest temperature [6, 40]. Power-law creep is an important mechanism that dominates maximum compressive stress at intermediate temperatures [41]. It's noted that only coble creep or constrained GB diffusional creep doesn't satisfactorily match the experiment results in this work, because both mechanism leads to an extremely fast stress relaxation and thus a very low stress at HT [9, 17], while in this work the stress in HT keeps nearly stable. A more precise mechanism is needed.

3.2 Warpage comparison of composites

The experiment results of measured warpage evolution of all sets are shown in Fig. 5, and warpage augment caused by PI is presented in Table 2. It's found that PI increases overall warpage at RT, and three results are concluded (Table 3).

Firstly, overall warpage can be estimated by Cu plus PI, and Cu contributes a substantial proportion of overall warpage. PI layers can enlarge warpage no matter it serves as a bottom buffer layer or as a surficial passivation layer. In fact two kind of PI shows ignorable curvature difference at RT, although the warpage evolution differs a lot at HT. It's somewhat counterintuitive to find that PI exacerbates overall wafer warpage, rather than reducing it as a soft visco substrate, as compared with *set B* and *set D.*

Secondly, warpage augment is mainly related to PI preparation history (i.e., the 1st PI layer or the 2nd PI layer) rather than PI/Cu relative position (bottom PI or surficial PI). From *set B* to *set C*, the 1st PI leads to 0.062 m^{-1} curvature augment, while from set D to set E, the curvature augment caused by the 2nd PI is only 0.03 m^{-1}.

Thirdly, mutual effect is observed. Warpage increasement caused by surficial PI (0.062 m^{-1}as from set B to set C) is slightly larger than bottom PI (0.056 m^{-1}as from set B to set D), but smaller than bare PI (0.071 m^{-1}, set A), suggesting that stress evolution of Cu and PI are somewhat restrained by each other.

4 Discussion

4.1 Stress distribution with PI joining

PI increases warpage at RT but decreases the stress of Cu. It's difficult to measure or analytically calculate the stress distribution in each layer of the composite, instead a simplified 2-dimensional axisymmetric FEA (finite element analyses) is conducted. The stress at RT can be regarded as generated by cooling from a reference temperature T_{ref} at which the warpage is zero (i.e., without stress within the composite). It's assumed that all layers at T_{ref} is also fully stress relaxed.T_{ref} is chosen at which the simulated warpage is equal to experimental value at RT. In a temperature range from RT to T_{ref}, PI and Cu and PI/Cu composites can be roughly considered as linear elastic, as demonstrated in Figs. 4 and 5. Geometric parameters are the same with experimental values except wafer radius is shrank to 5 mm.

The von-Mises stress of Cu films of line L_r in r direction, and normal stress of line L_z in z direction, are displayed in Fig. 6a, b respectively. The line L_r and L_z is depicted as insets in both figures. The von-Mises stress is derived from the center of Cu film, along from wafer center to the edge, and the normal stress is derived from the line that vertical to the wafer near the edge.

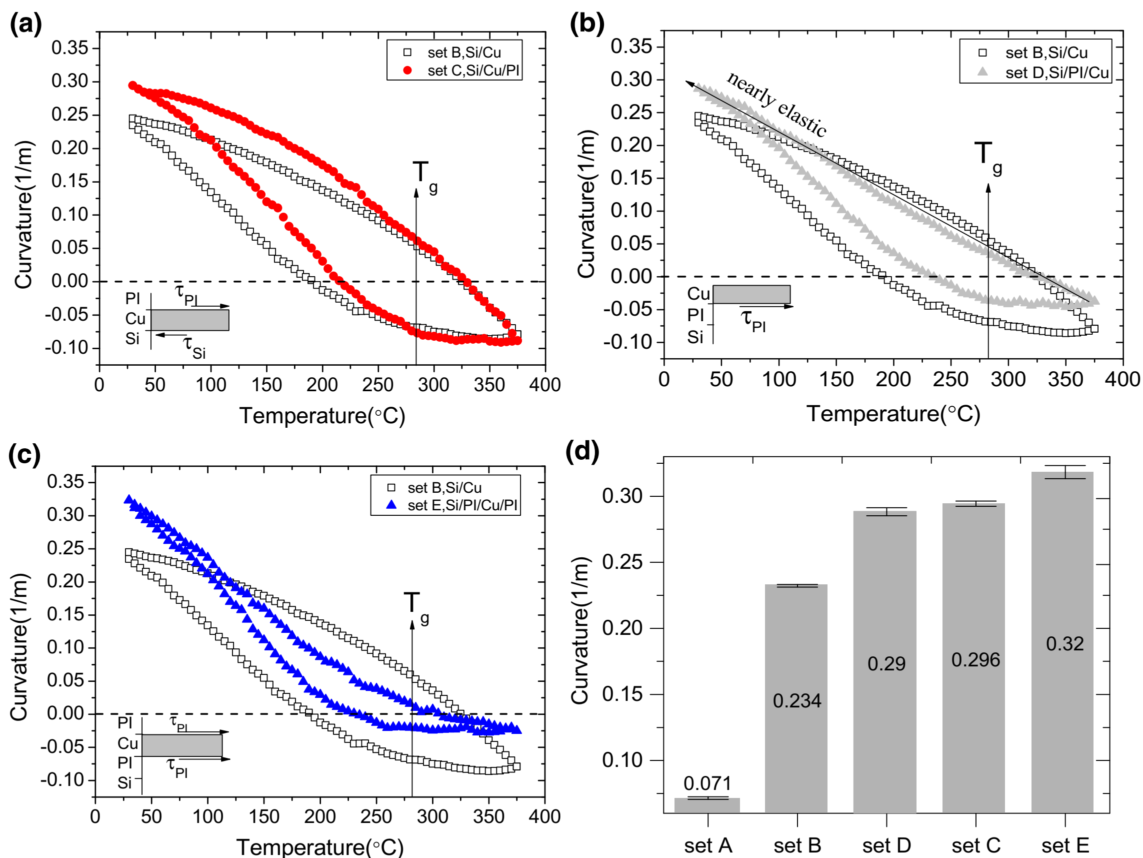

Fig. 5 The measured warpage evolution. **a**–**c** displays comparison of $\kappa - T$ response between bare Cu and Cu/PI composites, and **d** plots the warpage at RT of all sets, with the *I-shape* on the *top of the bar* indicating measuring error

Table 3 Warpage augment caused by PI

PI sequence	Bare PI	1st PI layer		2nd PI layer	
Relative position		Surficial PI	Bottom PI	Surficial PI	Bottom PI
Sample no.	A	B → C	B → D	D → E	C → E
Warpage augment (m^{-1})	0.071	0.062	0.056	0.03	0.024
Average	0.071	0.059 ± 0.003		0.027 ± 0.003	

It's clear that in both figures, the stress drops sharply from set B to set E, and multi PI layers leads to larger stress relaxation. The von-Mises stress in all sets generally decreases from wafer center to edge, and in the center area, PI leads to stress relaxation of Cu approximately by 6.26 % in *set C*, 10.27 % in *set D* and 21.91 % in *set E*. Figure 6b also indicates that the normal stress of Cu is slightly relaxed by 10.95 % by surficial PI in *set C*, but falls dramatically by 57.80 and 75.78 % with bottom PI joining in *set D and E* respectively.

The stress distribution is important for warpage evolution analyses. As is known, the spherical stress tensor can only change the volume of an object, and deviatoric stress tensor can cause the shape change and plastic deformation [42]. The von-Mises stress, from the second invariant of deviatoric stress tensor, determines shape change and deformation of Cu films in current work. Thus the von-Mises stress reduction will largely influence the warpage evolution, thermoelastic slope and hysteresis, as discussed below.

4.2 Hysteric loop and plasticity

Hysteresis, more or less resembling the internal friction, is a typical characteristics in $\sigma - \varepsilon$ plot of a metal film under biaxial stress with corresponding large plastic deformation, and hysteresis of $\kappa - T$ plot originates from $\sigma - \varepsilon$ plot. In fact, TSV wafers or thick films shows imperceptible hysteresis, because the triaxial stress gives rise to a relatively small effective shear stress required for plastic deformation

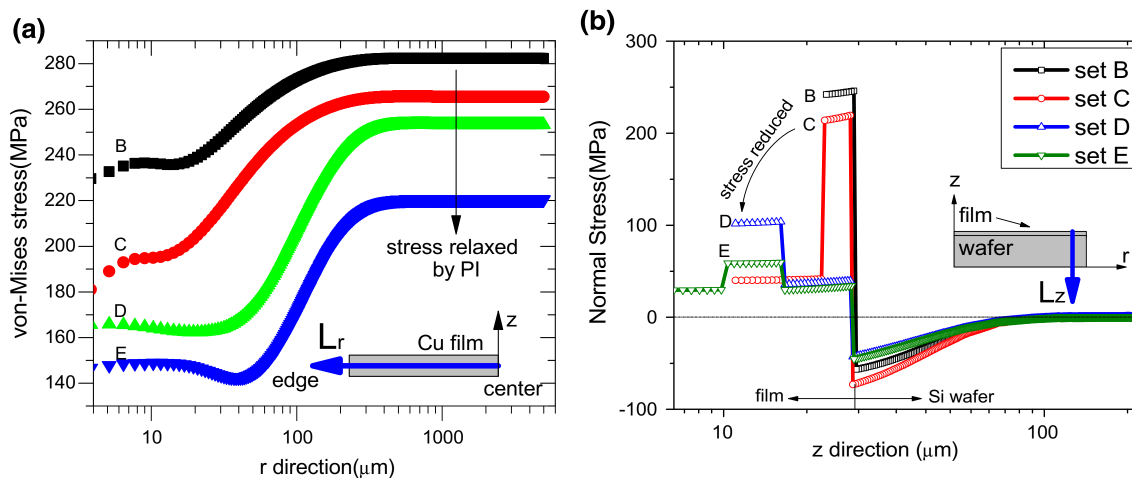

Fig. 6 The **a** von-Mises stress distribution of line L_r and **b** normal stress distribution of line L_z at RT by 2D axisymmetric FEA simulation. In **a**, L_r is along the center of the Cu film in r direction, and in **b**, L_z is vertical to the wafer and 20 μm far from wafer edge

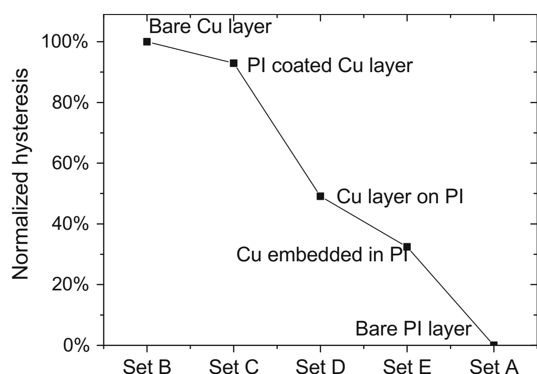

Fig. 7 The hysteresis is quantitated by loop area normalized by area of bare Cu film from *set B*

[35]. Besides, $\kappa - T$ plot from polymer films also shows ignorable hysteresis, as proved by PI in Fig. 4a. Accordingly, the hysteresis is a reflection of the von-Mises stress and plastic deformation of Cu. In current work, loop area normalized by the value of *set B* is applied to simply quantify the hysteresis, as exhibited in Fig. 7.

The hysteresis can be featured as three cases. Firstly, a closed loop means that the net deformation is basically zero after a thermal loading–unloading cycle, showing a pseudoelastic effect. Secondly, a stabilized and coincident loop during following cycles demonstrates a strong memory effect, indicating a thermal-stable-like state. Besides, the loop differs slightly with temperature loading rate during heating, proving that the mechanism is mainly temperature dominated rather than time dominated in current work.

Figure 7 evidently proves that PI suppresses hysteresis effectively, and multilayer of PI would lead to smaller loop area, suggesting smaller von-Mises stress and smaller plastic deformation in Cu. PI has different impact on hysteresis of Cu in different situations. A surficial PI layer in *set C* makes it 7 % smaller, while within a bottom PI it declines by 51 %, and two PI layers leads to a reduction of 68 %, which is in accordance with the result of FEA analyses of stress distribution of Cu in Fig. 6.

Generally, plastic deformation of Cu interconnect may cause lots of defects such as void or deterioration of conductivity, hence the electric performance of packaged devices may benefit from the hysteresis restraint.

5 Conclusion

In summary, five sets of composites are constructed to investigate the influence of PI on thermal stress evolution in Cu film by means of in situ wafer warpage measurement under thermal cycling. Combined with FEA and experimental results, it's found that PI reduces Cu stress but increases overall wafer warpage at RT. The hysteresis analyses indicate that PI reduces the overall plasticity of Cu, which may benefit for electric performance of Cu interconnection. It suggests that mutual effect should be considered when evaluating the stress distribution in polymer-metal composite thick films.

Acknowledgments This work was supported by National Natural Science Foundation of China (Grant Number NSFC61574154) and Natural Science Foundation of Shanghai (No. 13ZR1447300).

References

1. F. Brunner, A. Mogilatenko, A. Knauer et al., *J Appl Phys.* **112**(3), 033503 (2012)

2. H. J. Kim, S. C. Chong, D. S. W. Ho et al., in *2011 IEEE 61st Electronic Components and Technology Conference (Ectc)*, (2011), pp. 78–83
3. S.S. Deng, S.J. Hwang, H.H. Lee, IEEE Trans Comp. Pack Man **3**(3), 452–458 (2013)
4. N. P. Pham, M. Rosmeulen, G. Bryce et al., in *Proceedings of the 2012 IEEE 14th Electronics Packaging Technology Conference*, (2012), pp. 202–205
5. A. Tay, W. K. Ho, N. Hu et al., *Rev Sci Instrum.* **76**(7), 075111 (2005)
6. S.J. Hwang, Y.C. Joo, J. Koike, Thin Solid Films **516**(21), 7588–7594 (2008)
7. S.J. Hwang, Y.C. Joo, J. Koike, Thin Films-Stresses Mech. Prop. X **795**, 205–210 (2004)
8. E.S. Ege, Y.L. Shen, J. Electron. Mater. **32**(10), 1000–1011 (2003)
9. D. Weiss, H. Gao, E. Arzt, Acta Mater. **49**(13), 2395–2403 (2001)
10. R.M. Keller, S.P. Baker, E. Arzt, J. Mater. Res. **13**(5), 1307–1317 (1998)
11. S.P. Baker, A. Kretschmann, E. Arzt, Acta Mater. **49**(12), 2145–2160 (2001)
12. Y.L. Shen, U. Ramamurty, J. Appl. Phys. **93**(3), 1806–1812 (2003)
13. D. W. Gan, P. S. Ho, R. Huang et al., *J Appl Phys.* **97**(10), 103531 (2005)
14. E. Chason, J. W. Shin, S. J. Hearne et al., *J Appl Phys.* **111**(8), 083520 (2012)
15. H. Gao, L. Zhang, W.D. Nix et al., Acta Mater. **47**(10), 2865–2878 (1999)
16. D.W. Gan, P.S. Ho, Y.Y. Pang et al., J. Mater. Res. **21**(6), 1512–1518 (2006)
17. D. Chocyk, A. Proszynski, G. Gladyszewski, Microelectron. Eng. **85**(10), 2179–2182 (2008)
18. G. Dehm, M. Legros, B. Heiland, J. Mater. Sci. **41**(14), 4484–4489 (2006)
19. R. Schwaiger, G. Dehm, O. Kraft, Phil. Mag. **83**(6), 693–710 (2003)
20. B. von Blanckenhagen, E. Arst, P. Gumbsch, Acta Mater. **52**(3), 773–784 (2004)
21. W. Oh, T.J. Shin, M. Ree et al., Macromol. Chem. Phys. **203**(5–6), 801–811 (2002)
22. S.T. Chen, C.H. Yang, F. Faupel et al., J. Appl. Phys. **64**(12), 6690–6698 (1988)
23. D.M. Shinozaki, A. Klauzner, P.C. Cheng, Mater. Sci. Eng. Struct. **142**(1), 135–144 (1991)
24. I. Yadav, S. Dutta, A. Katiyar et al., Mater. Lett. **158**, 343–346 (2015)
25. M. Chao, K.C. Kou, G.L. Wu et al., J. Macromol. Sci. B **51**(10), 2003–2014 (2012)
26. M. Chao, K.C. Kou, G.L. Wu et al., J Macromol. Sci. A **49**(7), 578–585 (2012)
27. Y. Wang, K. Kou, G. Wu et al., Polymer **77**, 354–360 (2015)
28. Y.Q. Wang, K.C. Kou, W. Zhao et al., Rsc Adv. **5**(120), 99313–99321 (2015)
29. G.L. Wu, K.C. Kou, M. Chao et al., Thermochim. Acta **537**, 44–50 (2012)
30. G.L. Wu, K.C. Kou, L.H. Zhuo et al., Thermochim. Acta **559**, 86–91 (2013)
31. G. L. Wu, Y. H. Cheng, Q. Xie et al., *J. Polym. Res.* **21**(12), (2014)
32. G.L. Wu, K.C. Kou, N. Li et al., J. Appl. Polym. Sci. **128**(2), 1164–1169 (2013)
33. Y.H.C.G.L. Wu, K.K. Wang et al., J Mater. Sci.: Mater Electron. (2016). doi:10.1007/s10854-016-4464-y
34. R. Huang, D. Gan, P.S. Ho, J Appl Phys. **97**(10), 103532 (2005)
35. S.-K. Ryu, T. Jiang, K.H. Lu et al., Appl Phys Lett **100**(4), 041901 (2012)
36. C.S. Zhu, W.G. Ning, G.W. Xu et al., J. Electron. Mater. **43**(9), 3255–3262 (2014)
37. G.G. Stoney, Proc. R. Soc Lond A-Conta **82**(553), 172–175 (1909)
38. M.A. Hopcroft, W.D. Nix, T.W. Kenny, J. Microelectromech. S **19**(2), 229–238 (2010)
39. H. Ledbetter, E. Naimon, J. Phys. Chem. Ref. Data **3**(4), 897–935 (1974)
40. R.P. Vinci, E.M. Zielinski, J.C. Bravman, Thin Solid Films **262**(1–2), 142–153 (1995)
41. M.D. Thouless, J. Gupta, J.M.E. Harper, J. Mater. Res. **8**(8), 1845–1852 (1993)
42. Y. Huang, S. Qu, K.C. Hwang et al., Int. J. Plast. **20**(4–5), 753–782 (2004)